Reports

Lunar Gravity: The First Farside Map

Abstract. *A global lunar gravity field has been determined from data on the long-term motion of the Apollo 15 and Apollo 16 subsatellites and Lunar Orbiter 5. The nearside gravity map resolves major mascon basins and, in general, is in excellent agreement with the results of Muller and Sjogren. The farside gravity map is characterized by broad positive gravity in the highland regions with interspersed, localized, negative anomalies corresponding to major ringed basins. A comparison between global gravity and topography indicates that a thicker farside crust could be responsible for these gravitational differences between the two lunar hemispheres.*

Since the advent of the Lunar Orbiter missions, considerable effort has been devoted to the problem of finding an accurate representation for the lunar gravity field. Such a model would put needed surface constraints on the structure and composition of the lunar interior. The innovative work of Muller and Sjogren (*1*) led to the discovery of "mascons" and provided a consistent gravity map for the lunar nearside. Since that time the major problem has been how to determine the farside gravity from only nearside spacecraft tracking data (*2*). Earlier farside maps (*2, 3*) have had either unrealistic checkerboard patterns, have exhibited extraordinarily large variations, or were of such low order that possible correlation with surface topography was not evident. The Apollo era has provided a new wealth of gravity data over large regions of the moon from low altitudes. The largest contiguous block of low-altitude data consists of Doppler tracking data from the two Apollo subsatellites. These data, coupled with extended-mission Lunar Orbiter 5 data, constitute a comprehensive history of free fall and low-altitude sensing (20 to 200 km) covering 60 percent of the lunar sphere. Descriptions of each orbit are given in Table 1. This report presents the first plausible farside gravity map as derived from the long-term perturbations in the orbits of these satellites. I believe the essential breakthrough in this analysis is the application of a long-term selenodesy method to a high-resolution arc of Kepler element variations as provided by the Apollo subsatellites and Lunar Orbiter (*4*).

The raw data used were Doppler tracking data acquired by either the Manned Space Flight or the Deep Space Networks. In the case of the subsatellites, most data were obtained on the basis of one orbit per day during their active lifetimes. The block of Lunar Orbiter data used was acquired during every other orbit. The tracking data were reduced by least-squares fitting (*5*), and a set of mean Kepler elements $\bar{k}$ was obtained for every orbit during which Doppler data were acquired (*6*). Analyses have shown that all the assumptions made during this part of the data reduction result in the following position errors for the satellite: a radial error of 0.30 km, an along-track error of 3.0 km, and an out-of-orbit error of 3.0 km.

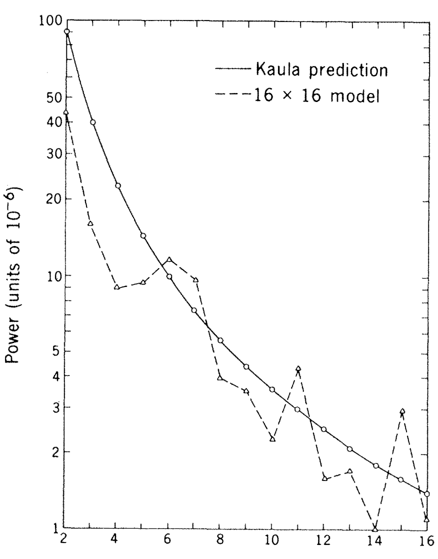

Fig. 1. Power spectrum of gravity coefficients.

The next step in the data reduction is to extract the long-term Kepler element rates from the history of mean elements. In order to accomplish this, each orbital element is considered as an independent function of time (*7*). The time derivatives of each set of Kepler elements (four-vector) are the long-term perturbing accelerations acting on the satellite. The derived rates are adjusted for *n*-body and solar radiation effects (*8*) such that only the variations due to lunar gravity remain. The first-order Lagrange equations (*9*) are used to relate the element rates ($\dot{\bar{k}}$) to the associated Kepler elements. This relationship is given as follows:

$$\dot{\bar{k}} = F(\bar{k})\,\bar{p}$$

where $\bar{p}$ is the vector of the harmonic coefficients of the lunar gravity potential. These equations are linear in the parameters to be estimated, and a least-squares solution can be used. The solution algorithm has the following well-known form (*10*):

$$\bar{p} = (F^{\mathrm{T}}\, W^{-1} F + \Gamma^{-1})^{-1} (\bar{p}^{*} + F^{\mathrm{T}}\, W^{-1}\, \dot{\bar{k}})$$

where W is a weighting matrix for each set of elements rates (assumed diagonal) and Γ is the a priori covariance associated with initial estimates $\bar{p}^*$ of the harmonics. In order to enhance the numerical stability of the least-squares solution, the square-root form (*11*) of these equations was used. The a priori statistics (*12*) for generating Γ were those given by Kaula (*13*) and the a priori estimates of $\bar{p}^*$ were assumed to be zero.

A 16th-degree, 16th-order harmonic solution was extracted from 266 sets of Keplerian rates (1064 data points). This representation contains spectral frequencies whose half-wave resolution is 11.25° on the lunar surface (341 km at the equator). Approximately 87 percent of the information has been extracted from the data with the use of this model. The data noise is calculated to be at the 95 percent level; the 8 percent difference between this model and noise represents the effect of unmodeled gravity terms above the 16th degree. The spectrum (*14*) for the harmonic coeffi-

Scoreboard for Reports: In the past few weeks the editors have received an average of 57 Reports per week and have accepted 12 (21 percent). We plan to accept about 10 Reports per week for the next several weeks. In the selection of papers to be published we must deal with several factors: the number of good papers submitted, the number of accepted papers that have not yet been published, the balance of subjects, and length of individual papers.

Authors of Reports published in *Science* find that their results receive good attention from an interdisciplinary audience. Most contributors send us excellent papers that meet high scientific standards. We seek to publish papers on a wide range of subjects, but financial limitations restrict the number of Reports published to about 12 per week. Certain fields are overrepresented. In order to achieve better balance of content, the acceptance rate of items dealing with physical science will be greater than average.

Table 1. Orbit description; ϕ, lunar latitude; λ, lunar longitude.

Satellite	Period	Eccen-tricity	Incli-nation	Data arc used	ϕ_{max}*	λ_{max}†
Apollo 15	2^h	0.02	151°	270^d	± 27°	0 to 360°
Apollo 16	2^h	0.02	170°	34^d	± 10°	0 to 360°
Lunar Orbiter 5	3^h	0.28	85°	9^d	± 40°	± 50°

*Maximum latitude coverage at or below 200 km. †Maximum longitude coverage at or below 200 km.

cients of this model and the Kaula prediction are shown in Fig. 1. For the lower-degree terms (degrees 2 through 4) the prediction appears to be too large by a factor of 2. The higher-degree terms in the spectrum agree in the mean with the prediction. The variation of the higher-degree spectrum (when considered on an individual degree basis) from the a priori value is a good indication of the independence of the solution from these nominal conditions.

Radial accelerations (in milligals) generated by this gravity field are evaluated at a 100-km reference altitude. Variations relative to a central body acceleration are shown in Figs. 2 and 3 for the lunar nearside and farside, respectively (*15*). A comparison of the lunar nearside as given by this model with results obtained using the line-of-sight acceleration method (*16*) shows very good agreement (*17*). This model resolves all five major nearside ringed basins (Maria Imbrium, Serenitatis, Crisium, Nectaris, and Humorum) as regions of strong positive gravity. Sinus Aestuum, Sinus Medii, and Grimaldi are also resolved as positive anomalies. Potential new anomalies are detected in the Aristarchus plateau region and in the southeastern highlands (30°S and 60°E). Mare Orientale is resolved as a near-circular negative anomaly, which is in agreement with the integrated effect as given by direct modeling (*18*). The mascon at Mare Smythii is not resolved. Minor differences between the actual location of smaller features and those given by the model can be attributed to the inability of the 16th-degree harmonics to resolve higher-degree effects.

The farside gravity map, in contrast to the nearside gravity map, is characterized by broad positive gravity regions in the highlands with interspersed, localized, negative anomalies over most of the major ringed basins. Prominent basins such as Mendeleev, Moscoviense, Korolev, and Apollo are all strong negative (−97 mgal or more) anomalies. Another strong localized negative anomaly (−99 mgal) corresponds to an unnamed smaller basin at 10°N and 205°E as identified by Apollo laser altimetry (*19*). Other farside ringed basins such as Hertzsprung, Ingenii, Gagarin, and Tsiolkovsky are relative lows in regions of gravity highs. All farside highland regions sampled by Apollo laser altimetry (*19*) are positive broad anomalies. When the gravity results shown in Figs. 2 and 3 are averaged (for 171 samples in each lunar hemisphere), the following statistical results are obtained: $\Delta g = +6 \pm 67$ mgal for the nearside and $\Delta g = +22 \pm 84$ mgal for the farside. This calculation suggests that, despite the presence of the mascons, the farside lunar gravity may be stronger than the nearside.

The strong positive (195 mgal) gravity anomaly centered near 5°N and 175°E has a topographic correspondence with a possible mascon basin (Mare Occultum) reported by Campbell *et al.* (*20*). Laser altimetry, however, shows this region to be upland terrain. Consequently, it seems probable that the origin of this gravity anomaly is related to the excess topography rather than to basalt floods. Another similar correlation exists between an anomaly at the northernmost extension of

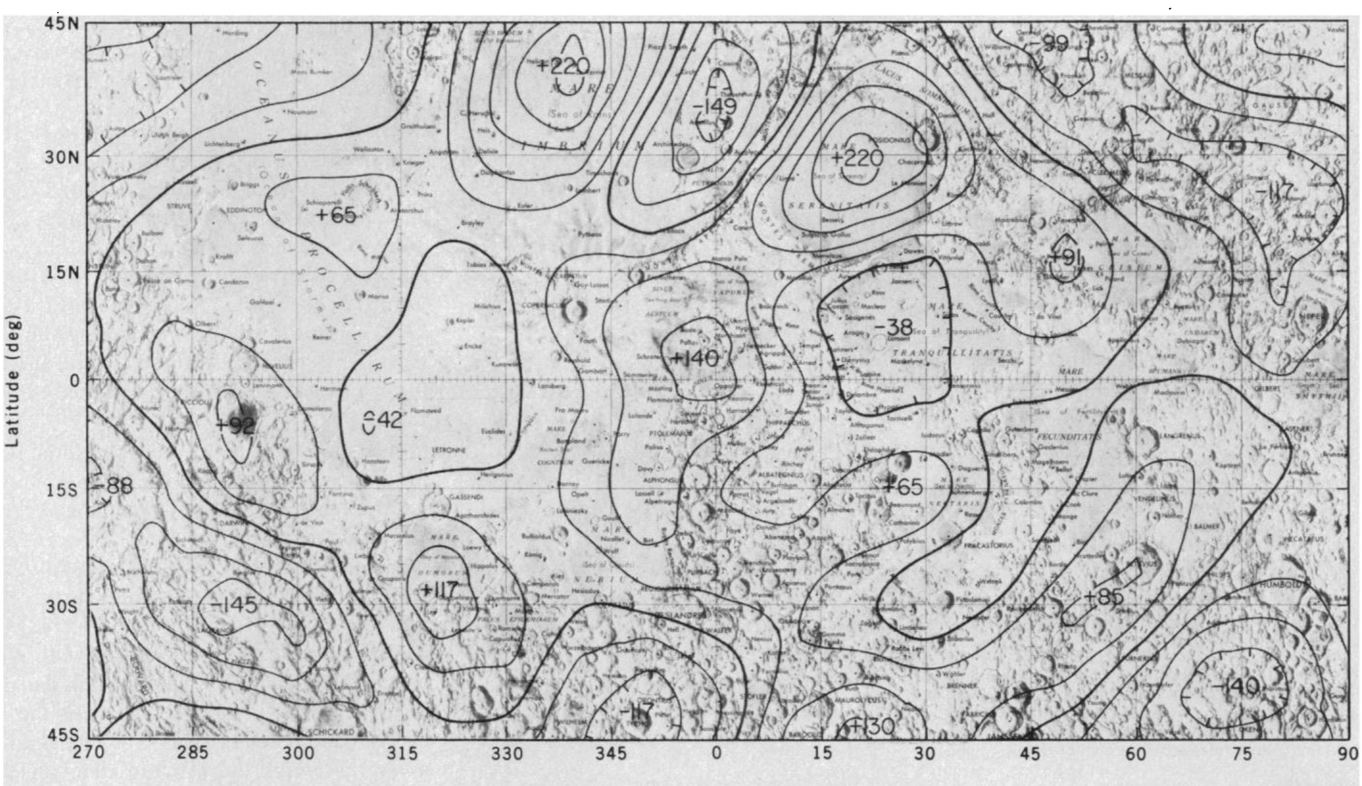

Fig. 2. Radial accelerations at an altitude of 100 km for the lunar nearside.

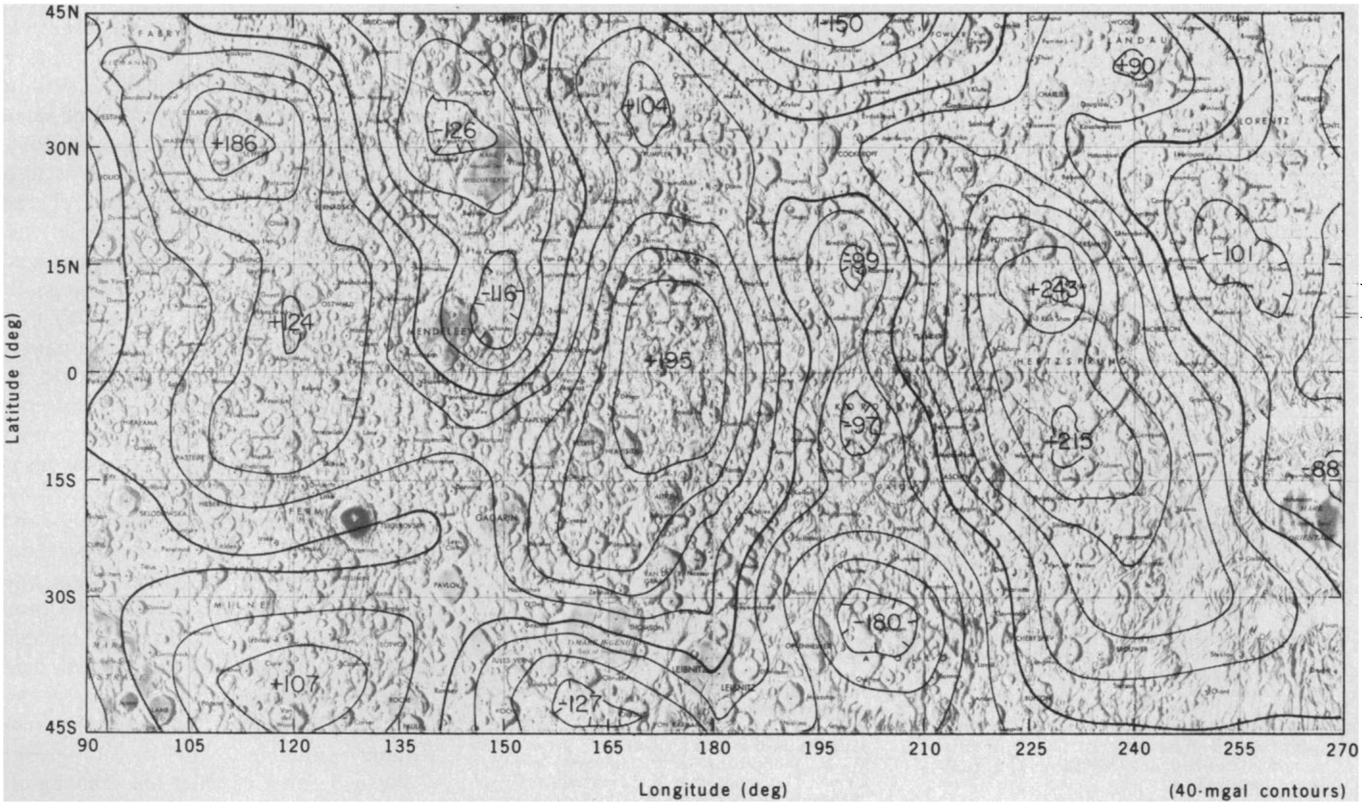

Fig. 3. Radial accelerations at an altitude of 100 km for the lunar farside.

the eastern farside highlands (+186 mgal) (30°N and 110°E) and a second suggested farside basin (Mare Marginis) as reported at that time (*20*). Although no direct measurements of topography are available over this region, an examination of the Apollo 15 and Apollo 16 altimetry (*19*) reveals a definite north-south trend for the highlands in this area. Consequently, it seems probable that topography is the cause of this anomaly also.

The filled ringed basins on the nearside are mascons, whereas unfilled ringed basins on the farside are negative anomalies. On the basis of this global gravity map and the associated topography, some rather interesting speculations can be made regarding the two lunar hemispheres. Laser altimetry (*19*) shows the major nearside flooded basins to be at elevations ranging from 1 to 4 km below the mean radius. Farside topography shows the preponderance of the regions sampled to be highlands whose elevations are 3 to 6 km above the mean radius. This topographic asymmetry, which exists about the center of mass of the moon, can be interpreted as a thicker farside crust (*21*). If it is assumed that basalts flowed until a state of hydrostatic equilibrium was reached, then the nearside basins, being topographically closer to the center of mass, were filled. Those basins on the farside, being further displaced, either remained completely unfilled or attained only a very slight filling. As a result, farside ringed basins are negative gravity anomalies, whereas nearside ones of equivalent size are mascons.

Accurate topographic data are available over only two of the major farside ringed basins, Mendeleev and Hertzsprung, which are also resolved by this gravity model. Using these data, I made a topographic correction to the observed (free-air) gravity to determine the Bouguer anomaly. Calculations were carried out for Mendeleev only since the regional characteristics of the topography surrounding Hertzsprung are very complex, requiring analysis beyond the scope of this report. Mendeleev is a depression of approximately 4 km (approximately 300 km in diameter) relative to the local topography with an observed gravity of -116 mgal. If a first-order topographic correction is made (*22*), the resulting Bouguer anomaly is +100 mgal. This result indicates that some degree of isostatic compensation in the lunar crust took place after basin formation. If an isostatic model is postulated consisting of a mantle plug (with a density of 3.35 g/cm^3 as compared to a surrounding density of 2.95 g/cm^3) of thickness 29.5 km at a depth of 70 km below the surface (*23*), the observed gravity at 100 km is -93 mgal. This model then shows that the state of isostatic rebound is almost complete for Mendeleev and is an indication of the viscoelastic properties of the lunar crust as a response to basin impact. In order to formulate a comprehensive model of crustal response to large impacts, many different features must be studied in detail as the gravity and topography data become available. Furthermore, data taken over unfilled basins could lead to a near-unique (*24*) geophysical model for the nearside mascons.

In future work more complex models (*25*) will be used to improve the resolution of known nearside features, and hopefully to identify new smaller-scale farside features.

ALFRED J. FERRARI
California Institute of Technology, Pasadena 91125

References and Notes

1. P. M. Muller and W. L. Sjogren, *Science* **161**, 680 (1968).
W. H. Michael, Jr., and W. T. Blackshear, *Moon* **3**, 388 (1972).
3. J. Lorell, *ibid.*, p. 190; A. S. Liu and P. A. Laing, *Science* **173**, 1017 (1971); W. L. Sjogren, *J. Geophys. Res.* **76**, 7021 (1971).
4. Although other researchers have used similar long-term selenodesy methods on Lunar Orbiter data, as of this time, no one, to my knowledge, has used both the Apollo subsatellite and Lunar Orbiter data as a combined data set.
5. These data were processed by a least-squares orbit determination scheme in which the assumed dynamical model includes the effects of a simple lunar potential model (harmonic coefficents: $C_{20} = -0.207108 \times 10^{-3}$, $C_{22} = 0.207 \times 10^{-4}$, $C_{30} = 0.21 \times 10^{-4}$, $C_{31} = 0.35 \times 10^{-4}$, and $C_{33} =$

0.258×10^{-5}) and the perturbing effects of the earth, sun, and solar radiation pressure. Tracking data from one nearside pass were used in the orbit determination. I obtained a best mean orbit from the Doppler data by differentially correcting estimates of the satellite position and velocity.
6. The satellite position and velocity are numerically integrated over one orbital period and simultaneously transformed to generate a history of five osculating Kepler elements (a, the semimajor axis; e, eccentricity; I, inclination; Ω, the longitude of the ascending node; and ω, the argument of the perifocus). These osculating elements are averaged over one orbital period to generate a set of mean elements.
7. Each element was fitted with patched cubic polynomials to smooth the data and permit the determination of an accurate time derivative. Analysis shows this method to be very accurate, and the errors introduced are shown to be well within the noise level of the mean elements. Since the time derivative of a due to long-term lunar perturbations is zero, it is not included in the calculation.
8. J. Lorell and A. S. Liu, *Jet Propulsion Lab. Rep. 32-1513* (1971); Y. Kozai, *Smithsonian Inst. Rep. 56* (1961).
9. W. M. Kaula, *Theory of Satellite Geodesy* (Blaisdell, Waltham, Mass., 1966), pp. 29–41.
10. A. P. Sage, *Optimum Systems Control* (Prentice-Hall, Englewood Cliffs, N.J., 1968), pp. 269–277.
- G. J. Bierman, *Inst. Electr. Electron. Eng. Trans. Aerosp. Electron. Syst.* **28**, 28 (1973).
12. I derived these statistics by scaling uncertainties in the gravity harmonics of the earth to those of the moon by assuming that each body can support equal stresses.
13. W. M. Kaula, *Science* **166**, 1581 (1969).
14. The spectrum for each degree of the gravity field is found from the following relationships involving the normalized harmonic coefficients $\bar{C}_{\ell m}, \bar{S}_{\ell m}$ (ℓ-degree, m-order):

$$\sigma_\ell^2 = \sum_{m=0}^{\ell} (\bar{C}_{\ell m}^2 + \bar{S}_{\ell m}^2)$$

$$S_\ell = \sigma_\ell (2\ell + 1)^{-1/2}$$

where σ_ℓ^2 is the variance of the ℓth degree and S_ℓ is its spectrum.
15. These accelerations contain all the spherical harmonic coefficients in the 16th-degree, 16th-order model.
16. P. M. Muller and W. L. Sjogren, *Appl. Mech. Rev.* **22** (No. 9), 955 (1969).
17. In the line-of-sight acceleration method a nominal potential model is used for orbit reduction. Line-of-sight accelerations given by this method represent deviations from this model. The quantitative effect of this reference potential is difficult to evaluate.
- W. L. Sjogren, R. W. Wimberly, W. R. Wollenhaupt, *Moon* **9**, 115 (1974).
19. W. L. Sjogren and W. R. Wollenhaupt, *Science* **179**, 275 (1973).
- M. J. Campbell, B. T. O'Leary, C. Sagan, *ibid.* **164**, 1273 (1969).
21. W. M. Kaula, G. Schubert, R. E. Lingenfelter, W. L. Sjogren, W. R. Wollenhaupt, *Geochim. Cosmochim. Acta* **3**, (Suppl. 3), 2189 (1972); E. M. Shoemaker, personal communication.
22. The gravity generated from a cylinder of thickness t, density ρ, and radius r at a field point a distance d away is given by:

$$\Delta g = 2\pi G\rho t\left[1 - \frac{d}{(d^2 + r^2)^{1/2}}\right]$$

where G is the universal constant of gravitation.
23. W. M. Kaula, G. Schubert, R. E. Lingenfelter, W. L. Sjogren, W. R. Wollenhaupt, *Geochim. Cosmochim. Acta* **3**, (Suppl. 5), 3049 (1974).
24. R. J. Phillips, *J. Geophys. Res.* **79**, 2027 (1974).
25. A limited set of higher-degree harmonic solutions will be attempted in the future. A parallel analysis is currently being pursued by M. Ananda of the Jet Propulsion Laboratory, using a discrete point mass modeling algorithm. A hybrid solution consisting of lower-degree harmonics and point masses will also be attempted.
26. The mean orbital elements for the Apollo subsatellites used in this analysis were generated by W. R. Wollenhaupt of the Johnson Spacecraft Center. I am indebted to N. E. Hamata and R. N. Wimberly of the Jet Propulsion Laboratory for their programming and computer assistance. I am also indebted to W. L. Sjogren of the Jet Propulsion Laboratory for his suggestions and support during this investigation. Contribution No. 2554 of the Division of Geological and Planetary Sciences, California Institute of Technology, Pasadena 91125.

23 December 1974; revised 21 February 1975

Psi Particles and Dyons

Abstract. *A hypothetical magnetic model of matter provides a natural setting for the newly discovered psi particles. This supplements a phenomenological description of such particles that had appeared prior to their experimental recognition.*

The first issue of *Physical Review Letters* in 1975 contained nine theoretical contributions that were snap-judgment responses to the dramatic discovery of new particles with unusual properties (*1*). Of these, only one (*2*) cited a previously published (*3*) anticipation of particles with the observed general characteristics (normal electromagnetic coupling and suppressed hadronic interaction). Such particles had been postulated in an attempt to supply a phenomenological (*4*) interpretation for the striking absence of hypercharge-changing neutral processes in the weak interactions, as unified with electromagnetism. By and large, the other letters in that issue proposed various speculative models for the new particles. I have written elsewhere (*5*) of the importance of maintaining a clear distinction between phenomenology and speculation in particle physics. My own contribution was purely phenomenological in character. But, as I have also noticed, thanks to the cool responses of individuals and audiences, phenomenology seems not to be enough; a speculative model is considered superior, or at least more interesting, no matter how logically inconsistent it may be. Accordingly, here is my speculation.

An article published a number of years ago in these pages (*6*) described a predominantly electromagnetic model of the subnucleonic world. It was based upon the concept of symmetry between electric and magnetic fields, as embodied in certain hypothetical spin ½, Fermi-Dirac particles, called dyons, that carry both electric and magnetic charges. These charges independently occur as fractional multiples, ⅔, −⅓, and −⅓, of the corresponding units of pure charge. All hadrons thus far known are considered to be magnetically neutral composites of dyons. The neutral combination of three dyons, with the respective magnetic charges ⅔, −⅓, and −⅓, is a Fermi-Dirac particle and a baryon, while a pairing of dyon with antidyon of the same magnitude of magnetic charge is a Bose-Einstein particle and a meson. It is also imagined, paralleling the electric charge exchange mediated by weak interactions, that magnetic charge is rapidly exchanged among the dyon constituents of a magnetically neutral hadron, in such a way that even a quite short time average of a particular dyon's magnetic charge would be zero. And it was pointed out, consistently with the previous remark, that conflict with the Fermi-Dirac statistics of dyons is avoided for the low-lying states of baryons, which seem to be symmetrical in space and spin variables, by invoking the physical degree of freedom of magnetic charge and placing these quantum numbers in a total antisymmetric state. Incidentally, this idea resurfaced later (*7*) with the physical identification in terms of magnetic charge deleted, and an empty, but sexy label substituted—color.

We have now reached the jumping-off point. Through the mechanism of rapid magnetic charge exchange, magnetically neutral hadronic systems acquire an approximate dynamical symmetry that can be expressed as an invariance with respect to a group of operations on the three-valued magnetic charge indices. The group has the structure of the unitary group in three dimensions, U_3. The total antisymmetry remarked on for low-lying hadrons is an invariance of these states under the special subgroup SU_3(mag.). That such states are not invariant under the full group U_3(mag.), but form one-dimensional representations of it, expresses their possession of the property of nucleonic charge, as commented on in (*6*). The low-lying mesons, which do not carry nucleonic charge, are invariant under the full magnetic group. It is now natural to envisage the existence of excited states that are not invariant under SU_3(mag.) but constitute members of certain multiplets, which are analogous to, but distinct from the SU_3 multiplets that are familiar in connection with the electric charge quantum numbers. To the extent that U_3(mag.) invariance is an accurate one, transitions between SU_3 (mag.)-invariant and -noninvariant states will occur slowly. Hence we identify the 1^- neutral particles ψ(3.1 Gev) and ψ(3.7 Gev) as members of a noninvariant magnetic multiplet.

The eight-dimensional representation that presents itself for mesons is labeled by magnetic analogs of isotopic spin T and hypercharge Y. Of the various pairs